Journal of Inorganic and General Chemistry
ZAAC
Zeitschrift für anorganische und allgemeine Chemie
DOI: 10.1002/zaac.202100146
ARTICLE

Structures and Properties of the Halogenido Stannates(II) [BMIm][Sn_3Cl_7] and [BMIm][Sn_4Br_9]

Mareike Liebertseder,[a] Silke Wolf,[a] and Claus Feldmann*[a]

Dedicated to Professor Josef Breu on the occasion of his 60th birthday.

The halogenido stannates(II) [BMIm][Sn_3Cl_7] and [BMIm][Sn_4Br_9] are obtained by ionic-liquid-based synthesis with SnX_2 and [BMIm]X (X=Cl, Br; [BMIm] = 1-butyl-3-methylimidazolium) near room temperature (45–50 °C). Both form colorless, moisture-sensitive crystals and exhibit layered anionic networks. [BMIm][Sn_3Cl_7] contains "horseshoe"-like $_\infty^1(SnCl_{1/1}Cl_{2/2})$ chains that are linked via $[SnCl_3]^-$ anions to $_\infty^2[Sn_3Cl_7]^-$ zigzag-planes. [BMIm][Sn_4Br_9] contains a complex $_\infty^2[Sn_4Br_9]^-$ network with altogether four different crystallographic Sn^{2+} sites and different coordination. For comparison with these complex halogenido stannates(II), $PbCl_2$/$PbBr_2$ are reacted with similar conditions, which, however, only results in [BMIm][$PbCl_3$] containing $_\infty^1[PbCl_3]^-$ chains. Beside the crystal structures, the thermal and optical properties are examined and feature certain emission of visible light for all title compounds at room temperature. Whereas the quantum yields of [BMIm][Sn_4Br_9] (3 %) and [BMIm][$PbCl_3$] (21 %) are low, [BMIm][Sn_3Cl_7] shows surprisingly efficient photoluminescence with a quantum yield of 46 %.

1. Introduction

Halogenido stannates(II) are known for their great structural variability, ranging from isolated $[SnX_3]^-$ and $[SnX_4]^{2-}$ anions (X=Cl, Br, I) via infinite chains with tetrahedral or square pyramidal building units to plane-like arrangements of edge- and corner-sharing octahedra.[1] In regard of infinite one-dimensional (1D) or two-dimensional (2D) building units, far the most examples were described for iodido stannates(II).[2] In the case of bromido stannates(II), the structural variability is much more limited, for instance, including the composition $M[Sn_2Br_5]^-$ (M=Rb, In) with infinite 2D networks.[3] A ring-type Sn_4Br_4 moiety was described in $RbSn_2Br_5$, in which Sn···Sn interactions occur.[4] Furthermore, a 2D network of $SnBr_6$ octahedra was observed in $[C_8H_{12}N]_2[SnBr_4]$.[5] Although the largest number of compounds is known for chlorido stannates(II), they show lower structural variability in regard of infinite anionic networks than the respective bromides and iodides. Thus, isolated $[SnCl_3]^-$,[6] $[SnCl_4]^{2-}$,[7] and $[Sn_2Cl_5]^-$[6c,8] anions were observed most frequently. Expanded Sn–Cl building units also consist of these anions and are linked via long-ranging interactions in few cases.[9] Thus, the compound $[Ni(CH_3CN)_6](Sn_2Cl_5)(SnCl_3)\times 0.5CH_3CN$ shows long-ranging interactions between $[Sn_2Cl_5]^-$ with $[SnCl_3]^-$ anions.[9a] In $K_{2-2x}Sn_{5+x}Cl_{12}$ as a sole example of expanded Sn–Cl building units, infinite $_\infty^1[SnCl_2]$ chains are linked via long-ranging interactions and K^+ cations to form a 3D network.[9b] Finally, it needs to be mentioned that halogenido stannates(II), and specifically iodido stannates(II), recently became interesting to replace iodido plumbates(II) as so-called perovskite-type solar absorbers.[10]

Because of the different ionicity of tin(II) halides, the solubility of the starting materials is significantly different from each other. Whereas SnI_2 shows good solubility in many organic solvents, $SnBr_2$ is only soluble in the most polar organic solvents (e.g., dimethylsulfoxide/DMSO, dimethylformamide/DMF), in which $SnCl_2$ is also nearly insoluble. To address the limitation of the low solubility, ionic liquids turned out to be a suitable alternative. Since both $SnCl_2$ and $SnBr_2$ are weak Lewis acids, they can react with organo halides [Cation]X to pseudo-ternary compounds [Cation][SnX_3] or [Cation][Sn_2X_5], which instantaneously represent ionic liquids ([Cation], e.g. 1-butyl-3-methylimidazolium/[BMIm], X=Cl, Br).[6c] Such Lewis-acidic ionic liquids – most often $AlCl_3$-based systems – have already shown great potential for the preparation of new compounds that can be hardly obtained in conventional solvents.[11] Some recent examples include, for instance, the intermetalloid $[CuBi_8]^{3+}$ cluster cation in $[CuBi_8][AlCl_4]_2[Al_2Cl_7]$,[12] the highly coordinated $Sn(II)I_8$ subunit in the carbonyl $[SnI_8\{Fe(CO)_4\}_4][Al_2Cl_7]_2$,[13] the $[Sb_{10}Se_{10}]^{2+}$ cation in $[Sb_{10}Se_{10}][AlCl_4]_2$,[14] or the heavy-metal porphyrin-analogue $[Hg_4Te_8(Te_2)_4]^{8-}$ in $[DMIm]_8[Hg_4Te_8(Te_2)_4]$ ([DMIm]$^+$ = 1-decyl-3-methylimidazolium).[15] Aiming at expanded Sn–Cl or Sn–Br networks, syntheses in ionic liquids could also be a promising strategy.[6c,16] As a result, we here present the novel halogenido stannates(II) [BMIm][Sn_3Cl_7] (**1**), [BMIm][Sn_4Br_9] (**2**), as well as the halogenido plumbate(II) [BMIm][$PbCl_3$] (**3**).

[a] Dr. M. Liebertseder, Dr. S. Wolf, Prof. Dr. C. Feldmann
Institut für Anorganische Chemie
Karlsruhe Institute of Technology (KIT)
Engesserstraße 15, D-76131 Karlsruhe (Germany)
Phone: (+)49-721-60842855
E-mail: claus.feldmann@kit.edu
Homepage: http://www.aoc.kit.edu

Supporting information for this article is available on the WWW under https://doi.org/10.1002/zaac.202100146

2. Results and discussion

2.1. Ionic-liquid-based synthesis

[BMIm][Sn_3Cl_7] (**1**) and [BMIm][Sn_4Br_9] (**2**) were both prepared by ionic-liquid-based synthesis near room temperature (45–50 °C) using $SnCl_2$/$SnBr_2$ and [BMIm]Cl/[BMIm]Br as starting materials. Both title compounds were obtained as colorless needles with yields of 60–70 %. In regard of the conditions of the reaction, it must be noticed that only the crystallization of $SnCl_2$/$SnBr_2$ was observed at higher temperatures. At lower temperatures, the title compounds were also formed, but with significantly smaller crystal size and lower yield. For **1** and **3**, $AlCl_3$ was added to obtain [BMIm][$AlCl_4$] as ionic liquid and to increase the solubility of $SnCl_2$ and $PbCl_2$. Furthermore, it must be noticed that **1** was only obtained in the presence of SnO. In absence of SnO, only a yellowish ionic liquid with non-dissolved $SnCl_2$ was obtained. $AlCl_3$ as a strong Lewis acid obviously activates SnO by the formation of soluble Al–O–Cl species[17] and allows the Sn:Cl ratio to become independent from 1:2 adjusted by $SnCl_2$ only. To verify the reactions of $SnCl_2$/$SnBr_2$, we have tried to react $PbCl_2$/$PbBr_2$ with similar conditions. Various attempts, however, only resulted in [BMIm][$PbCl_3$] (**3**), which was synthesized by reacting $PbCl_2$, [BMIm]Cl, and $AlCl_3$. **3** was obtained as colorless rhomboids after three weeks at 50 °C.

2.2. Structural characterization

[BMIm][Sn_3Cl_7] (**1**) crystallizes in the non-centrosymmetric space group *Ia* (Table 1) and consists of non-charged $_\infty^1(SnCl_{1/1}Cl_{2/2})$ zigzag-chains, which are linked by $[SnCl_3]^-$ anions to infinite anionic layers (Figure 1a). These layers are separated from each other by $[BMIm]^+$ cations. The $_\infty^1(SnCl_{1/1}Cl_{2/2})$ zigzag-chains are folded in a way that they look like "horseshoes" (Figure 2a). These horseshoe-like chains are oriented with all open sides of the horseshoe in the same direction, which can be considered to be the origin of the non-centrosymmetric symmetry (Figure 2a). In these $_\infty^1(SnCl_{1/1}Cl_{2/2})$ chains, Sn^{2+} is threefold pyramidally coordinated by three chlorine atoms. Two of them are each connecting to two tin atoms (256.3(3)–274.5(3) pm, Table 2). Taking a closer look at the connecting chlorine atoms reveals two sets of shorter (256.3(3), 261.0(3) pm) and longer Sn···Cl (273.7(3), 274.5(3) pm) distances. These values fit well with binary $SnCl_2$ (266.4, 278.2 pm).[18] The additional two chlorine atoms (Cl6, Cl7) are terminally bound (244.0(3), 247.8(2) pm). These distances are as well in agreement with terminally bound Sn(II)–Cl arrangements (e.g. 245.6–248.8 pm in [PPh_4][$SnCl_3$]).[6b] Finally, long-ranging interactions occur in the $_\infty^1(SnCl_{1/1}Cl_{2/2})$ zigzag-chain for Sn3···Cl7 (327.7(4) pm) (Table 2, Figure 2a), which compare to [$Co(CH_3CN)_6$][$SnCl_3$][Sn_2Cl_5]×0.5 CH_3CN (long-ranging Sn···Cl distances up to 330.2 pm).[9,18]

Table 1. Crystallographic data and refinement details of [BMIm][Sn_3Cl_7] (**1**), [BMIm][Sn_4Br_9] (**2**), and [BMIm][$PbCl_3$] (**3**).

Compound	1	2	3
Sum formula	$C_8H_{15}N_2Cl_7Sn_3$	$C_8H_{15}N_2Sn_4Br_9$	$C_8H_{15}N_2PbCl_3$
Crystal system	Monoclinic	Monoclinic	Orthorhombic
Space group	*Ia**	$P2_1/c$	*Pnma*
Lattice parameters	a = 992.4(2) pm	a = 1457.8(1) pm	a = 792.8(1)
	b = 1998.0(4) pm	b = 2225.5(1) pm	b = 979.9(1)
	c = 1062.5(2) pm	c = 816.9(1) pm	c = 1732.0(3)
	β = 104.9(1)°	β = 102.6(1)°	
Cell volume V	2036.2×10^6 pm^3	2586.6×10^6 pm	1345.6×10^6 pm
Formula units per cell	Z = 4	Z = 4	Z = 4
Calculated density ρ	2.425 g/cm^3	3.423 g/cm^3	2.235 g/cm^3
Measurement limits	$-13 \le h \le 13$,	$-20 \le h \le 20$,	$-10 \le h \le 9$,
	$-27 \le k \le 27$,	$-31 \le k \le 31$,	$-13 \le k \le 11$,
	$-14 \le l \le 14$	$-11 \le l \le 9$	$-23 \le l \le 23$
2 Theta range for data collection	4.1 to 58.8°	3.2 to 70.7°	4.7 to 58.7°
Wavelength	Mo–K_α	Ga–K_α	Mo–K_α
	(λ = 0.71073 Å)	(λ = 1.34013 Å)	(λ = 0.71073 Å)
Linear absorption coefficient μ	4.561 mm^{-1}	31.612 mm^{-1}	13.102 mm^{-1}
Number of reflections	9833	36032	11828
	(5186 independent)	(7552 independent)	(1911 independent)
Refinement method	Full-matrix least-squares on F^2	Full-matrix least-squares on F^2	Full-matrix least-squares on F^2
Merging	R_{int} = 0.053	R_{int} = 0.039	R_{int} = 0.032
Number of parameters	184	210	108
Residual electron density	−1.14 to 1.22 e^- 10^{-6} pm^{-3}	−3.58 to 2.34 e^- 10^{-6} pm^{-3}	−2.30 to 0.92 e^- 10^{-6} pm^{-3}
Figures of merit	R1 ($I \ge 4\sigma_I$) = 0.037	R1 ($I \ge 4\sigma_I$) = 0.040	R1 ($I \ge 4\sigma_I$) = 0.029
	R1 = 0.042	R1 = 0.066	R1 = 0.035
	wR2 (all data) = 0.104	wR2 (all data) = 0.084	wR2 (all data) = 0.076
	GooF = 1.099	GooF = 1.082	GooF = 1.088

(* Flack parameter: −0.04(3) indicates the absence of inversion twinning)

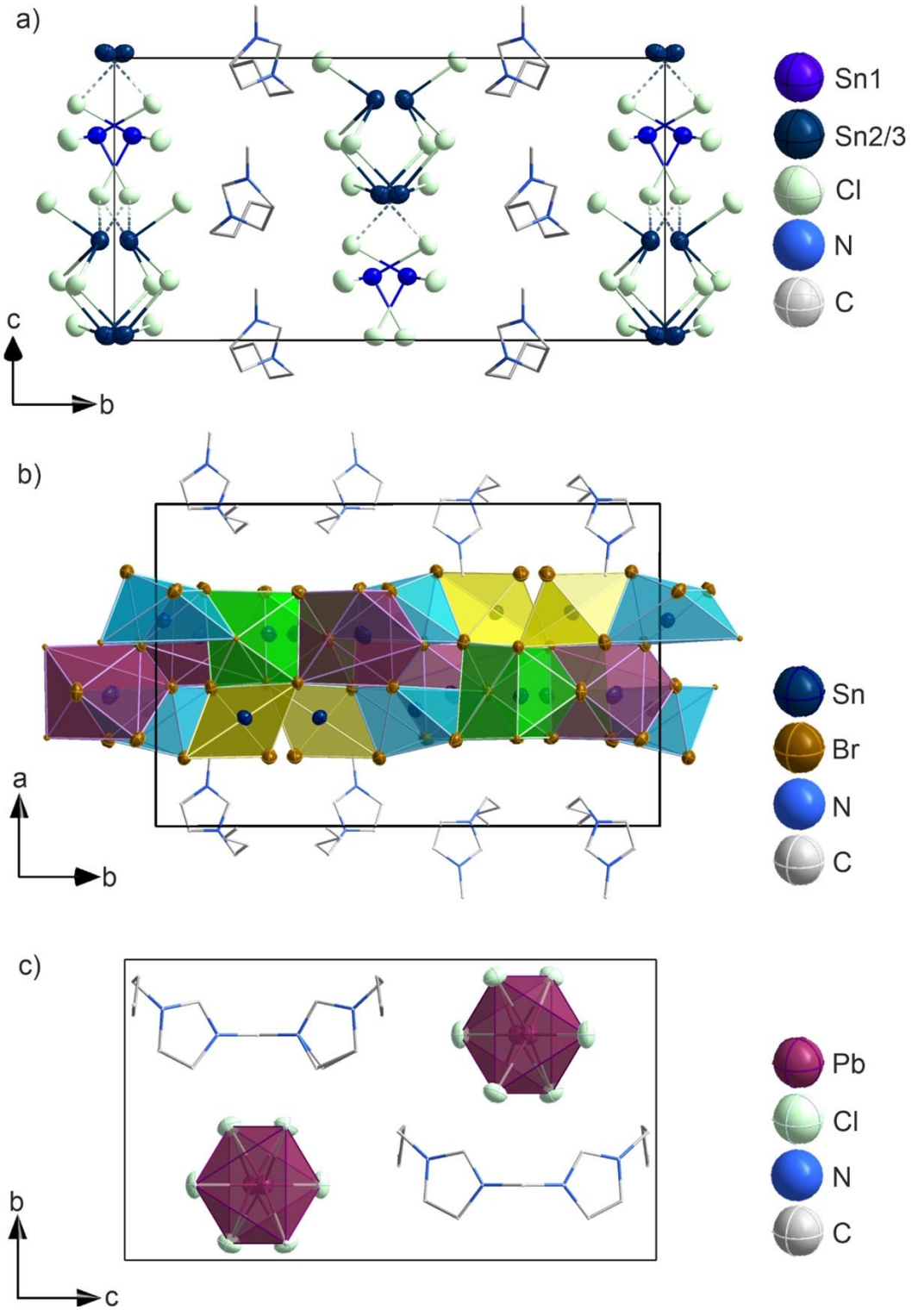

Figure 1. Unit cells of $[BMIm][Sn_3Cl_7]$ (**1**), $[BMIm][Sn_4Br_9]$ (**2**) with different $SnBr_n$ polyhedra indicated by different colors, and $[BMIm][PbCl_3]$ (**3**).

The $_\infty^1(SnCl_{1/1}Cl_{2/2})$ zigzag-chains are further linked via long-ranging interactions with $[SnCl_3]^-$ anions (Figure 2b). These pyramidal $[SnCl_3]^-$ anions exhibit Sn–Cl distances of 251.3(3) and 255.1(3) pm and Cl–Sn–Cl angles of 87.6(1)° to 90.7(1)° (Table 2). Both is well in agreement with literature data (e.g. $K_2SnCl_4 \times H_2O$: Sn–Cl of 254 and 263 pm, Cl–Sn–Cl angles of 88 and 91°).[6a] Long-ranging distances occur between Cl atoms of $[SnCl_3]^-$ and Sn atoms of the $_\infty^1(SnCl_{1/1}Cl_{2/2})$ chains (299.8(4),

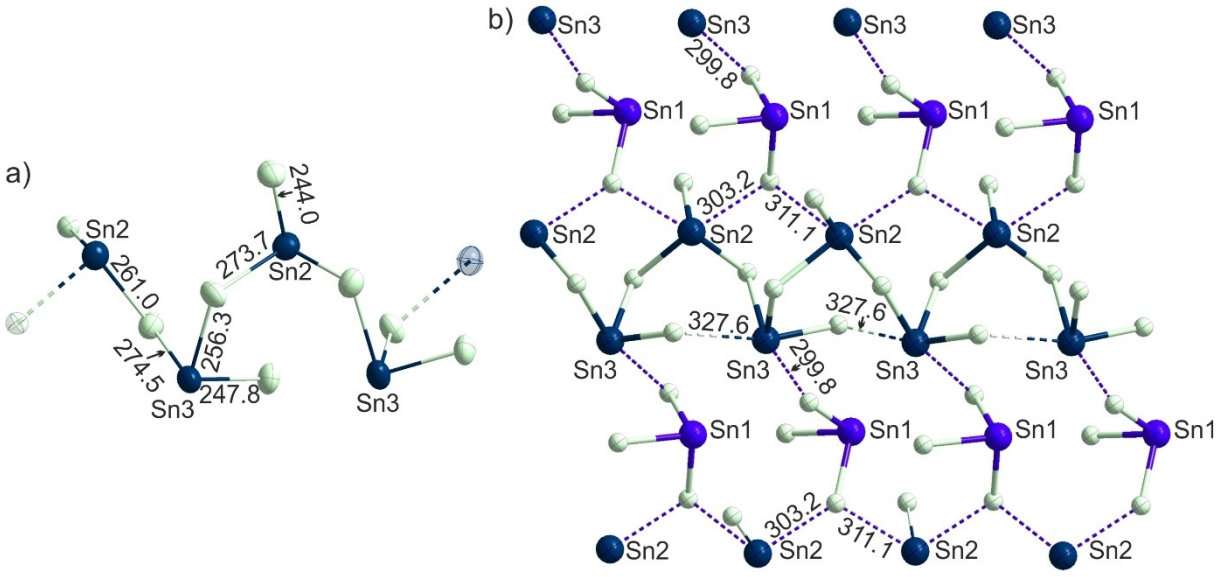

Figure 2. Structural features of [BMIm][Sn_3Cl_7] (**1**): a) $_{\infty}^{1}[SnCl_{1/1}Cl_{2/2}]^-$ chain, b) linkage of $_{\infty}^{1}[SnCl_{1/1}Cl_{2/2}]^-$ chains to $_{\infty}^{2}[Sn_3Cl_7]^-$ zigzag-planes.

Table 2. Sn–Cl, Sn–Br and Pb–Cl distances (in pm) in [BMIm][Sn_3Cl_7] (**1**), [BMIm][Sn_4Br_9] (**2**), and [BMIm][$PbCl_3$] (**3**) in comparison to literature data.

Compound	Coordination number	Distance/pm
1	Sn1: 3	251.1(3), 252.1(3), 255.1(3)
	Sn2: 3	244.0(3), 261.0(3), 273.7(2)
	Sn3: 3	247.8(2), 256.3(2), 274.5(3)
$SnCl_2$[18]	9	266.4, 278.2 (2×), 305.8 (2×), 321.9, 330.2, 385.2 (2×)
$[PPh_4][SnCl_3]$[6b]	3	245.6, 246.7, 248.8
$NaSn_2Cl_5$[16]	Sn1: 8	254.6, 272.8 (2×), 306.8 (2×), 359.1 (2×), 372.9
	Sn2: 9	256.3, 259.6 (2×), 319.2, 332.5 (2×), 392.9 (2×), 405.9
2	Sn1: 4	266.2(1), 273.8(1), 287.4(1), 318.0(1)
	Sn2: 5	273.8(1), 287.4(1), 291.4(1), 316.7(1), 319.4(1)
	Sn3: 5	269.2(1), 277.7(1), 299.4(1), 305.1(1), 322.8(1)
	Sn4: 6	269.3(1), 300.1(1), 306.0(1), 312.3(1), 317.3(1), 336.0(1)
$SnBr_2$[20]	8	281.4, 291.9 (2×), 315.8 (2×), 338.7
$Rb[Sn_2Br_5]$[4]	4	275.5(2×), 310.5(2×)
3	6	268.7(2), 270.5(1) (2×), 311.7(1), 314.7(1) (2×)
$PbCl_2$[23]	9	279.5, 290.8 (2×), 304.4 (2×), 303.5, 308.9, 370.2 (2×)
$[(R)–C_8H_{12}N][PbCl_3]$[22]	6	268.9, 273.7, 282.2, 294.8, 313.4, 321.9

311.1(4) pm), which are again in the expected range.[9,18] Even longer distances are observed between tin in $[SnCl_3]^-$ and terminally bound chlorine atoms of the $_{\infty}^{1}(SnCl_{1/1}Cl_{2/2})$ chains (Sn1···Cl6: 341.7(4), Sn1···Cl7: 349.0(4) pm). In sum, all these Sn–Cl interactions result in $_{\infty}^{2}[Sn_3Cl_7]^-$ layers (Figure 2b). These anionic layers are separated by $[BMIm]^+$ cations, which exhibit the expected distances and angles. Finally, moderate H···Cl bridge bonding occurs between $[BMIm]^+$ and the anionic $_{\infty}^{2}[Sn_3Cl_7]^{n-}$ layers with 267.8(3) pm.[19]

[BMIm][Sn_4Br_9] (**2**) crystallizes in the monoclinic space group $P2_1/c$ (Table 1). Herein, $[Sn_4Br_9]^-$ establishes an anionic $_{\infty}^{2}[Sn_4Br_9]^-$ network with $[BMIm]^+$ cations in between (Figure 1b). To visualize the structure, the crystallographically different Sn^{2+} sites are discussed separately. Altogether, **2** exhibits four different Sn^{2+} sites showing different types of coordination (Figure 3a). Sn1 is coordinated by four bromine atoms that form a strongly distorted tetrahedron with Sn–Br distances of 266.2(1)–318.0(1) pm (Table 2, Figure 3b). The coordination of Sn2 comprises five bromine atoms and a distorted square pyramidal polyhedron (Sn–Br: 273.8(1)–319.4(1) pm). Moreover, the long Sn2···Br2 distance (348.7(1) pm) needs to be included into the coordination environment (Table 2, Figure 3c). The Sn3 site is similar to Sn2 and also includes five bromine atoms with distorted square pyramidal coordination (Sn–Br: 269.2(1)–322.8(1) pm, Table 2, Figure 3d). Finally, Sn4 shows a distorted pentagonal pyramid as coordination polyhedron with six bromine atoms (Sn–Br: 269.0(1)–336.0(1) pm, Table 2, Figure 3e). All aforementioned

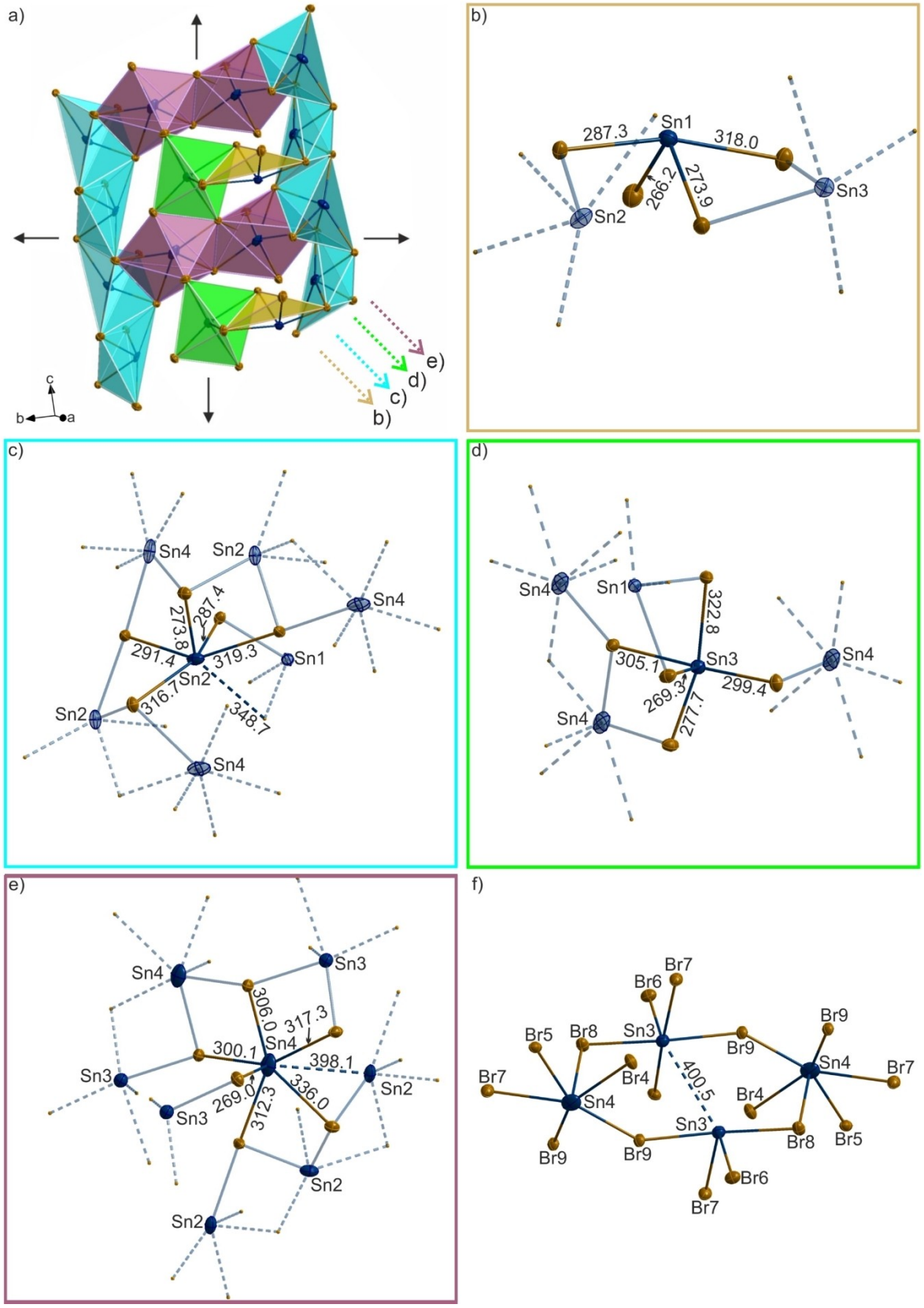

Figure 3. Structural features of [BMIm][Sn_4Br_9] (**2**) with $_{\infty}^{2}[Sn_4Br_9]^-$ network: a) overview of the different $SnBr_n$ polyhedra and their connectivity (Sn1: yellow, Sn2: blue, Sn3: green, Sn4: violet), b-d) coordination and distances of the different $SnBr_n$ polyhedra, f) Sn_4Br_4 ring formed by $SnBr_n$ polyhedra shown in (d) and (e).

Sn–Br distances in the $_{\infty}^{2}[Sn_4Br_9]^-$ network are in good agreement with the literature (281.4–338.7 pm).[20] All Sn^{2+} sites exhibit a clear influence of the stereochemically active lone-pair, which can be considered to be the origin of the variability of the Sn^{2+} coordination.

The different polyhedra in the $_{\infty}^{2}[Sn_4Br_9]^-$ network are connected via corner- and edge-sharing (Figure 3a). The square pyramids around Sn2 form chains via edge-sharing along the crystallographic *c*-axis. The polyhedra around Sn1, Sn3 and Sn4 are located between these chains, resulting in a planar arrangement in the crystallographic *b*,*c*-plane. Comparable 2D tin bromide networks were also reported for $RbSn_2Br_5$ or $InSn_2Br_5$.[3,4] However, the anionic network and coordination of **2** – to the best of our knowledge – was not observed before. A Sn_4Br_4-ring as observed for the Sn3 and Sn4 sites (Figure 3f) was also described in $InSn_2Br_5$,[4] where the authors point to short $Sn^{2+}\cdots Sn^{2+}$ distances (412.4(1) pm). This was ascribed to an interaction of the lone pair of one Sn^{2+} with the empty *d*-orbital of a neighbored Sn^{2+}. For **2**, we observe an even shorter $Sn^{2+}\cdots Sn^{2+}$ distance of only 398.1(8) pm (Sn2···Sn4).

$[BMIm][PbCl_3]$ (**3**) crystallizes in the orthorhombic space group *Pnma* and consists of $_{\infty}^{1}[PbCl_3]^-$ chains (Table 1, Figure 1c), which are separated by $[BMIm]^+$ cations. Here, it should be noticed that the $[BMIm]^+$ cation is disordered, which was tackled by split-atom positions with 50% probability of finding for all N/C atoms. The Pb–Cl distances range from 268.7(2) to 270.5(1) pm, which is in good agreement with literature data (268.9–294.8 pm).[22,23] In addition to these short Pb–Cl distances, longer distances of 311.7(1) to 314.7(1) pm are observed (Table 2). As a result, Pb^{2+} is coordinated by six chlorine atoms forming distorted octahedra with three shorter and three longer Pb–Cl distances (Figure 4a). These $PbCl_6$ octahedra are face-sharing, resulting in $_{\infty}^{1}[PbCl_{6/2}]^-$ chains (Figure 4b). Similar arrangements have been reported in the literature before (e.g. $[(R)C_8H_{12}N]PbCl_3$).[22,24,25] Please note that **3** is the only compound that we could obtain with comparable experimental conditions as applied for the synthesis of **1** and **2**.

2.3. Thermal and optical properties

Aiming at further material characterization and material properties, first of all, Fourier-transform infrared spectra were recorded (Figure 5). The spectra are dominated by vibrations of the

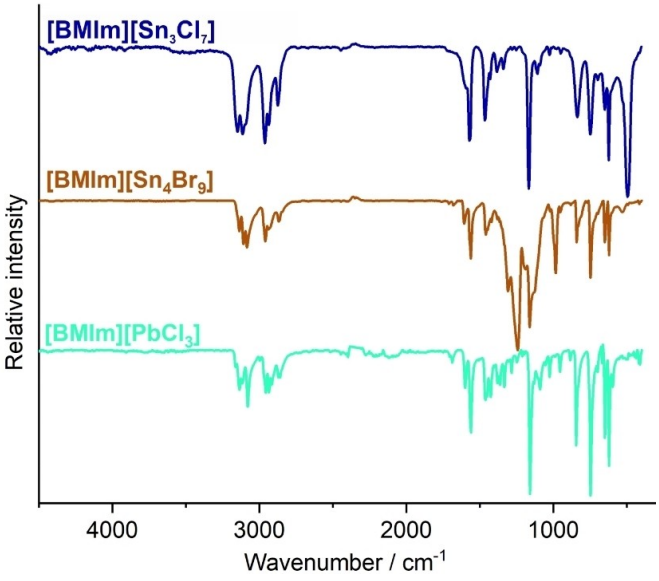

Figure 5. Infrared spectra of $[BMIm][Sn_3Cl_7]$ (**1**), $[BMIm][Sn_4Br_9]$ (**2**), and $[BMIm][PbCl_3]$ (**3**).

$[BMIm]^+$ cation (3147–2837, 1570, 1464, 1165 cm^{-1}). These vibrations are characteristic for the imidazolium cation. For **1**, the Sn–Cl vibration at 498 cm^{-1} is clearly visible (Figure 5), whereas the Sn–Br and Pb–Cl vibrations occur outside the measured range at low wavenumbers. Moreover, the lack of O–H- or C=O-related vibrations is indicative for the absence of oxide/hydroxide/carbonate impurities in the title compounds.

Thermogravimetry (TG) and differential thermal analysis (DTA) were used to examine the thermal properties of all title compounds (Figure 6). Accordingly, **1** shows an endothermic DTA peak related to the melting point at 240 °C. The compound starts to decompose at 350 °C with a single step and a total weight loss of 94.9% (Figure 6a). The decomposition can be ascribed to the decomposition of [BMIm]Cl and the evaporation of $SnCl_2$ (calculated: 100%). The observed minor remain (5.1%) can be ascribed by partial hydrolysis to SnO/SnO_2 over the duration of the experiment. **2** starts to decompose at 227 °C with a single step and a total weight loss of 79.1% (Figure 6b). Here, the decomposition can be related to the decomposition of [BMIm]Br and the evaporation of $SnBr_4$ stemming from the

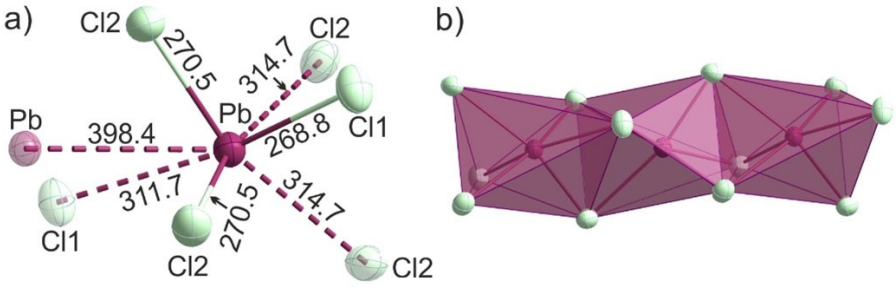

Figure 4. Structural features of $[BMIm][PbCl_3]$ (**3**): a) Pb–Cl coordination, b) $_{\infty}^{1}[PbCl_{6/2}]^-$ chain.

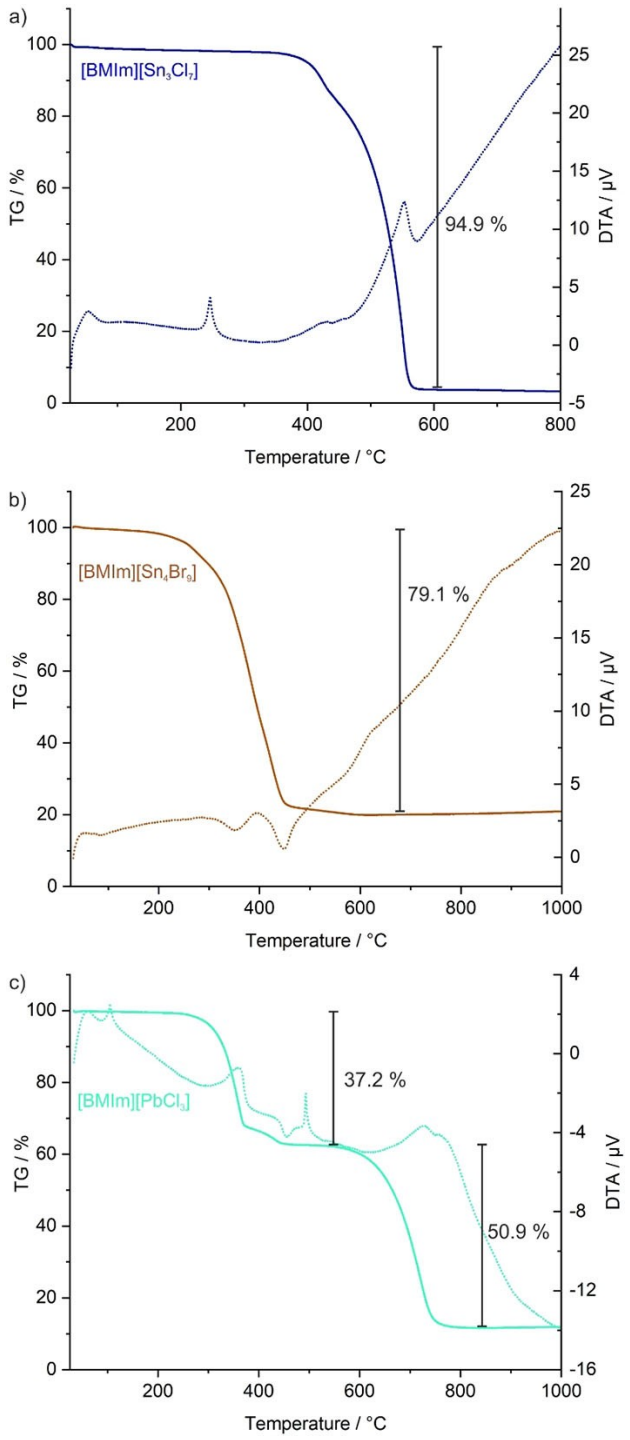

Figure 6. Thermogravimetry (solid line) and differential thermal analysis (dashed line) of a) $[BMIm][Sn_3Cl_7]$ (**1**), b) $[BMIm][Sn_4Br_9]$ (**2**), c) $[BMIm][PbCl_3]$ (**3**).

disproportionation of $SnBr_2$ (calculated: 82.2 %) with elemental tin remaining as solid residue (calculated: 17.8 %). Finally, **3** shows a melting point at 105 °C as well as a second endothermic DTA peak at 495 °C, which can be assigned to the melting point of $PbCl_2$ (Figure 6c). **3** starts to decompose at 250 °C in two steps with weight losses of 37.2 and 50.9 %. The first step can be assigned to the decomposition of [BMIm]Cl (calculated: 38.6 %). The second step is caused by the evaporation of $PbCl_2$ (calculated: 61.4 %). The difference in relation to the solid residue can be again assigned to partial hydrolysis and formation of PbO because of the long duration and the high temperature of the measurement.

Beside the thermal properties, the optical properties of the title compounds were studied. First of all, ultraviolet-visible (UV-Vis) spectroscopy was performed (Figure 7). Here, a steep absorption below 350 nm (**1**), 550 nm (**2**), and 450 nm (**3**) is observed due to valence-band-to-conduction-band excitation. The absorption is more-or-less similar to the binary halides $SnCl_2$, $SnBr_2$, $PbCl_2$ and only slightly blue-shifted. During UV-Vis spectroscopy, we realized that the title compounds also show visible emission (Figure 8), which was quantified by photoluminescence spectroscopy. The excitation spectra of **1** show strong absorption at 320–420 nm with a maximum at 379 nm (Table 3, Figure 8a). Excitation is followed by bluish-white emission at 350–650 nm with its maximum at 436 nm. This emission can be related to $5s^1p^1 \rightarrow 5s^2p^0$ transition on Sn^{2+}, which is also in accordance with the observed Stokes shift of about 100 nm.[26] Even though Sn^{2+}-based emission is known in principle, it is typically observed for Sn^{2+}-doped (1–5 mol-%) host lattice compounds (e.g., β-$Ca_3(PO_4)_2:Sn^{2+}$, $(Sr,Mg)_3(PO_4)_2:Sn^{2+}$).[27] At higher Sn^{2+} concentrations (> 10 mol-%), the emission is usually quenched by concentration quenching.[26,27] For **1**, the luminescence process is surprisingly efficient as expressed by an absolute quantum yield of 46 ± 3 % at room temperature (Table 3). This finding can be ascribed to the comparably large distance between the luminescent Sn^{2+} centers (≥ 386.2(2) pm) and the large size of the $[BMIm]^+$ cation. Such situation was similarly observed for compounds such as $[C_4N_2H_{14}Br]_4[SnBr_6]$ or $[C_9NH_{20}]_2[SnBr_4]$.[28] For the compounds **2** and **3**, weak emission of white and blue light was observed (Figure 8b,c). However, the quantum yield is significantly lower as compared to **1** with only about 3 % for **2** and 21 % for **3** (Table 3). The lower quantum yield of **2** and **3** is in accordance with a less rigid coordination of the larger bromine and lead in comparison to chlorine and tin, resulting in a higher contribution of loss processes driven by lattice defects and vibrational relaxation.

3. Conclusion

The halogenido stannates(II) $[BMIm][Sn_3Cl_7]$ and $[BMIm][Sn_4Br_9]$ were prepared via ionic-liquid-based synthesis near room temperature (45–50 °C) by reaction of SnX_2, $AlCl_3$ and [BMIm]*X*

Table 3. Excitation and emission maxima as well as quantum yield of $[BMIm][Sn_3Cl_7]$ (**1**), $[BMIm][Sn_4Br_9]$ (**2**), and $[BMIm][PbCl_3]$ (**3**).

Compound	Excitation/nm	Emission/nm	Quantum yield/%
1	369	436	46
2	350	383, 403	3
3	360	406	21

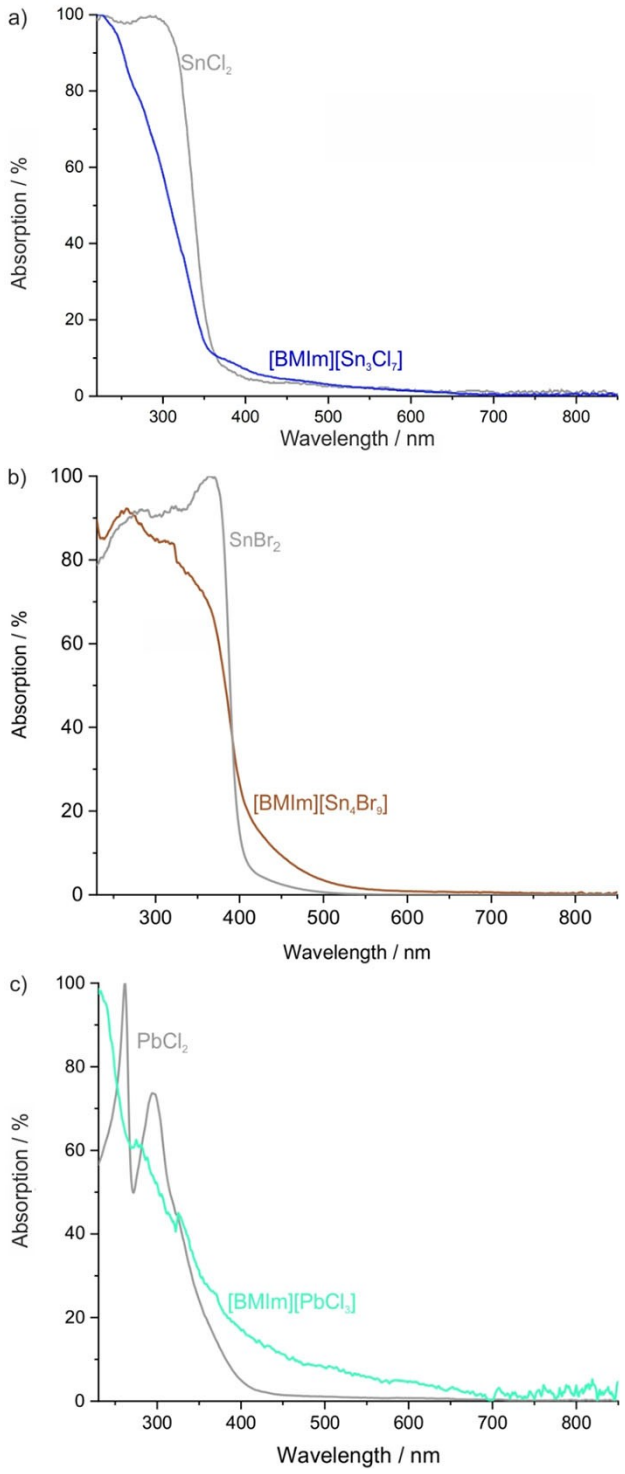

Figure 7. UV-Vis spectra of [BMIm][Sn_3Cl_7] (**1**), b) [BMIm][Sn_4Br_9] (**2**), c) [BMIm][$PbCl_3$] (**3**).

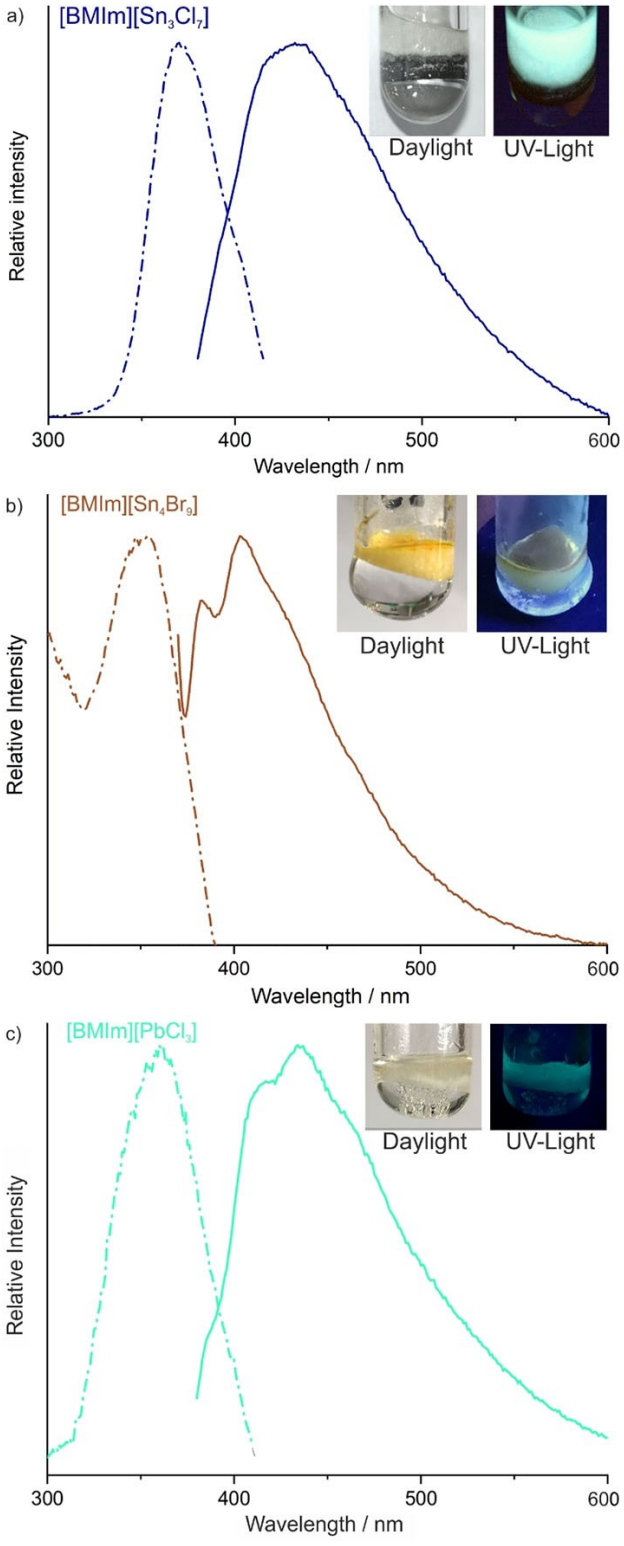

Figure 8. Excitation and emission spectra of a) [BMIm][Sn_3Cl_7] (**1**), b) [BMIm][Sn_4Br_9] (**2**), c) [BMIm][$PbCl_3$] (**3**) at room temperature with photos of the compounds in daylight and with excitation ($\lambda = 366$ nm) as insets.

(X=Cl, Br; [BMIm] = 1-butyl-3-methylimidazolium). Both compounds show complex layered anionic networks. Thus, [BMIm][Sn_3Cl_7] exhibits "horseshoe"-like $_{\infty}^{1}(SnCl_{1/1}Cl_{2/2})$ zigzag-chains that are linked via $[SnCl_3]^-$ to $_{\infty}^{2}[Sn_3Cl_7]^-$ zigzag-planes. [BMIm][Sn_4Br_9] contains a complex $_{\infty}^{2}[Sn_4Br_9]^-$ network with four different Sn^{2+} sites with different coordination. Similar syntheses with $PbCl_2$/$PbBr_2$ only resulted in [BMIm][$PbCl_3$] with

$_{\infty}^{1}[PbCl_3]^-$ chains. The synthesis in ionic liquids is beneficial due to the low synthesis temperature and the weakly coordinating properties of the solvent. Beside the realization of new compounds and novel structural features, all title compounds show emission of visible light at room temperature. The quantum yields of [BMIm][Sn_4Br_9] (3 %) and [BMIm][$PbCl_3$] (21 %) are limited, whereas [BMIm][Sn_3Cl_7] shows good photoluminescence with a quantum yield of at least 46 %.

Experimental

Material synthesis

General: All reactions and sample handling were carried out under dried argon atmosphere using standard Schlenk techniques and/or gloveboxes (MBraun Unilab, $c(O_2, H_2O) < 0.1$ ppm). Reactions were performed in Schlenk flasks and glass ampoules that were evacuated ($p < 10^{-3}$ mbar), heated, and flashed three times with Argon prior to use. The starting materials $SnCl_2$ (99.99 %, ABCR), $SnBr_2$ (99.5 %, Alfa Aesar), SnO (99 %, ABCR), $PbCl_2$ (95 %, VWR), and $AlCl_3$ (99.9 %, Sigma-Aldrich) were used as received. [BMIm]Cl (99 %, Iolitec) and [BMIm]Br (99 %, Iolitec) was dried under reduced pressure (10^{-3} mbar) at 130 °C for 48 h.

*Synthesis of [BMIm][Sn_3Cl_7] (**1**).* 100 mg (1 eq, 0.527 mmol) of $SnCl_2$, 71.0 mg of SnO (1 eq, 0.527 mmol), 300 mg (1.718 mmol) of [BMIm]Cl, and 35.2 mg (0.264 mmol) of $AlCl_3$ were heated under argon in a sealed glass ampoule for 3 weeks at 45 °C. This unusually long reaction time was required to obtain the title compound and suitable single crystals at low temperature. At higher temperatures, we only observed a recrystallization of $SnCl_2$. After cooling to room temperature, the title compound was obtained in the form of large colorless needles growing on top of undissolved SnO with a yield of about 55 % (calculated based on the amount of $SnCl_2$). After the reaction, the SnO phase can be clearly differentiated from the title compound, so that single crystals of **1** are easy to separate manually. **1** is very sensitive to moisture and needs to be strictly handled under inert conditions. Finally, it should be noticed that **1** was only obtained in the presence of SnO. This can be ascribed to the opportunity to obtain a Sn:Cl ratio different from 1:2 when using $SnCl_2$ only.

*Synthesis of [BMIm][Sn_4Br_9] (**2**).* 100 mg of [BMIm]Br (1 eq, 0.456 mmol), and 508 mg of $SnBr_2$ (4 eq, 1.82 mmol) were mixed in a glass ampoule and heated to 50 °C for 96 h. Subsequently, the reaction mixture was cooled to room temperature with a rate of 1 K/h. After cooling to room temperature, colorless needles of **2** were obtained as sole product with a yield of about 67 %. **2** is highly moisture sensitive and must be handled under inert conditions.

*Synthesis of [BMIm][$PbCl_3$] (**3**).* In a first step, the [BMIm][$AlCl_4$] as ionic liquid was synthesized by mixing of 100 mg (1 eq, 0.573 mmol) of [BMIm]Cl and 38 mg $AlCl_3$ (0.5 eq, 0.287 mmol) in an ampoule. After certain period in time, the two solids form [BMIm][$AlCl_4$] at room temperature. Thereafter, 79 mg (0.5 eq, 0.287 mmol) of $PbCl_2$ were added. The sealed ampoule was then heated to 50 °C for 96 h and subsequently cooled to room temperature with a rate of 1 K/h. After cooling to room temperature, phase-pure **3** was obtained with colorless rhomboedral crystals and a yield of about 73 %. **3** is highly moisture sensitive and has to be handled under inert conditions.

Analytical techniques

Crystal structure determination and refinement. For single crystal structure analysis, suitable crystals were selected manually, covered by inert-oil (perfluoropolyalkylether, ABCR), and deposited on a micro gripper (MiTeGen). Data collection of **1** and **3** was performed at 200 K on an IPDS II image-plate diffractometer (Stoe, Darmstadt) using Mo–K_α radiation ($\lambda = 0.71073$ Å, graphite monochromator). Data collection for **2**, which formed significantly smaller and even more sensitive crystals than **1** and **3**, was performed at 180 K on a Stoe StadiVari diffractometer with Euler geometry (Stoe, Darmstadt) using Ga–K_α radiation ($\lambda = 1.34013$ Å, graded multilayer mirror as monochromator).

Data reduction and multi-scan absorption correction were conducted by the X-AREA software package and STOE LANA (version 1.75).[29] Space group determination based on systematic absence of reflections was performed by XPREP. Using Olex2,[30] the structures were solved with the ShelXS[31] structure solution program with Direct Methods and refined with the ShelXL[31] refinement package using least squares minimization. All non-hydrogen atoms were refined anisotropically. Details of structure determination and structure refinement are listed in Table 1. DIAMOND was used for all illustrations.[32] Refinement was checked with PLATON.[33] Further details related to the crystal structures may be obtained from the joint CCDC/FIZ Karlsruhe deposition service on quoting the depository number 2077888 (**1**), 2077889 (**2**), and 2077890 (**3**).

Fourier-transform infrared (FT-IR) spectra were recorded on a Bruker Vertex 70 FT-IR spectrometer (Bruker). The samples were measured as pellets in KBr. Thus, 300 mg of dried KBr and 0.5–1.0 mg of the title compound were carefully pestled together and pressed to a thin pellet.

Thermogravimetry (TG) was carried out with a Netzsch STA 449 F3 Jupiter device using α-Al_2O_3 as crucible material and reference. Buoyancy effects were corrected by baseline subtraction of a blank measurement. The samples were measured under dried nitrogen up to 800 °C with a heating rate of 10 K/min. The Netzsch software PROTEUS Thermal Analysis (Version 5.2.1) was used for graphical evaluation.

Optical spectroscopy (UV-Vis) of powder samples was recorded on a Shimadzu UV-2700 spectrometer, equipped with an integrating sphere, in a wavelength interval of 250–800 nm against $BaSO_4$ as a reference.

Photoluminescence spectroscopy. Excitation and emission spectra were recorded using a photoluminescence spectrometer Horiba Jobin Yvon Spex Fluorolog 3, equipped with a 450 W Xenon lamp, double monochromator for excitation and emission, an integrating sphere (Ulbricht sphere) and a photomultiplier as the detector. The determination of the quantum yield was performed according to Friend *et al.*.[34] First of all, the diffuse reflection of the sample was determined under excitation conditions. Thereafter, the emission was measured at this excitation wavelength. Integration over the reflected and emitted photons with an Ulbricht sphere results in the absolute quantum yield. Corrections were made regarding the spectral power of the excitation source, the reflection behavior of the Ulbricht sphere, and the sensitivity of the detector.

Acknowledgements

The authors thank for the Deutsche Forschungsgemeinschaft (DFG) for funding in the Priority Program SPP1708 “Material synthesis near room temperature”. Moreover, we acknowledge

the Karlsruhe Nano Micro Facility (KNMF) and Prof. Dr. D. Fenske and Dr. A. Eichhöfer for data collection on a Stoe StadiVari diffractometer with Ga-metal-jet source.

Conflict of Interest

The authors declare no conflict of interest.

Keywords: Tin(II) · halide · ionic liquid · crystal structure · photoluminescence

[1] a) L. Apostolico, G. Kociok-Köhn, K. C. Molloy, C. S. Blackman, C. J. Carmalt, I. P. Parkin, *Dalton Trans.* **2009**, 10486–10494; b) C. Lode, H. Krautscheid, *Z. Anorg. Allg. Chem.* **2000**, *626*, 326–331; c) C. Lode, H. Krautscheid, *Z. Anorg. Allg. Chem.* **2007**, *633*, 1691–1694; d) C. Lode, H. Krautscheid, *Z. Anorg. Allg. Chem.* **2001**, *627*, 1454–1458.
[2] a) I. Chung, J.-H. Song, J. Im, J. Androulakis, C. D. Malliakas, H. Li, A. Freeman, J. Arthur J T Kenney, M. G. Kanatzidis, *J. Am. Chem. Soc.* **2012**, *134*, 8579–8587; b) J. L. Knutson, J. D. Martin, D. B. Mitzi, *Inorg. Chem.* **2005**, *44*, 4699–4705; c) S. Wang, D. B. Mitzi, C. A. Feild, A. Guloy, *J. Am. Chem. Soc.* **1995**, *117*, 5297–302.
[3] H. P. Beck, *Z. Anorg. Allg. Chem.* **1986**, *536*, 45–52.
[4] I. Abrahams, J. D. Donaldson, S. Grimes, G. Valle, S. Calogero, *Polyhedron* **1986**, *5*, 1593–1596.
[5] G. S. Lorena, H. Hasegawa, Y. Takahashi, J. Harada, T. Inabe, *Chem. Lett.* **2014**, *43*, 1535–1537.
[6] a) R. E. Rundle, D. H. Olson *Inorg. Chem.* **1963**, *3*, 596–598; b) U. Müller, N. Mronga, C. Schumacher, K. Dehnicke, *Z. Naturforsch.* **1982**, *37b*, 1122–1126; c) M. Currie, J. Estager, P. Licence, S. Men, P. Nockemann, K. R. Seddon, M. Swadźba-Kwaśny, C. Terrade, *Inorg. Chem.* **2013**, *52*, 1710–1721.
[7] H. J. Haupt, F. Huber, H. Preut, *Z. Anorg. Allg. Chem.* **1976**, *2*, 97–103.
[8] a) S. A. R. Bird, J. D. Donaldson, J. Silver, *J. Chem. Soc. Dalton Trans.* **1972**, 1950–1953; b) Z. Zhang, H. D. Lutz, *J. Solid State Chem.* **1995**, *115*, 158–164.
[9] a) M. Veith, B. Gdicke, V. Huch, *Z. Anorg. Allg. Chem.* **1989**, *579*, 99–110; b) H. P. Beck, H. Nau, *Z. Anorg. Allg. Chem.* **1988**, *558*, 193–200.
[10] a) S. D. Stranks, P. K. Nayak, W. Zhang, T. Stergiopoulos, H. J. Snaith, *Angew. Chem. Int. Ed.* **2015**, *54*, 3240–3248; *Angew. Chem.* **2015**, *127*, 3288–3297; b) M. Grätzel, *Nat. Mater.* **2014**, *13*, 838–842.
[11] a) E. Ahmed, M. Ruck, *Dalton Trans.* **2011**, *40*, 9347–9357; b) D. Freudenmann, S. Wolf, M. Wolff, C. Feldmann, *Angew. Chem. Int. Ed.* **2011**, *50*, 11050–11060; *Angew. Chem.* **2011**, *123*, 11244–11255; c) J. Dupont, *Acc. Chem. Res.* **2011**, *44*, 1223–1231.
[12] M. Knies, M. Kaiser, A. Isaeva, U. Mueller, Th. Doert, M. Ruck, *Chem. Eur. J.* **2018**, *24*, 127–132.
[13] S. Wolf, R. Köppe, T. Block, R. Pöttgen, P. W. Roesky, C. Feldmann, *Angew. Chem. Int. Ed.* **2020**, *59*, 5510–5514; *Angew. Chem.* **2020**, *132*, 5552–5556.
[14] E. Ahmed, A. Isaeva, A. Fiedler, M. Haft, M. Ruck, *Chem. Eur. J.* **2011**, *17*, 6847–6852.
[15] C. Donsbach, K. Reiter, D. Sundholm, F. Weigend, S. Dehnen, *Angew. Chem. Int. Ed.* **2018**, *57*, 8770–8774; *Angew. Chem.* **2018**, *130*, 8906–8910.
[16] A. P. Abbott, G. Capper, D. L. Davies, H. L. Munro, R. K. Rasheed, V. Tambyrajah, *Chem. Commun.* **2001**, *19*, 2010–2011.
[17] J. Richter, M. Ruck, *Molecules* **2020**, *25*, 78.
[18] J. M. van den Berg, *Acta Crystallogr.* **1961**, *14*, 1002–1003.
[19] a) T. Steiner, *Angew. Chem. Int. Ed.* **2002**, *41*, 48–76; *Angew. Chem.* **2002**, *114*, 50–80; b) G. A. Jeffrey, *An Introduction to Hydrogen Bonding*, Oxford University Press, Oxford 1997.
[20] I. Abrahams, D. Z. Demetriou, *J. Solid State Chem.* **2000**, *149*, 28–32.
[21] I. Abrahams, D. Z. Demetriou, R. T. Kroemer, H. Taylor, M. Motevalli, *J. Solid State Chem.* **2001**, *160*, 382–387.
[22] D. G. Billing, A. Lemmerer, *CrystEngComm* **2006**, *8*, 686–695.
[23] R. L. Sass, E. B. Brackett, T. E. Brackett, *J. Phys. Chem.* **1963**, *67*, 2863–2864.
[24] A. C. Véron, A. Linden, N. A. Leclaire, E. Roedern, S. Hu, W. Ren, D. Rentsch, F. A. Nüesch, *J. Phys. Chem. Lett.* **2018**, *9*, 2438–2442.
[25] Y. Deng, X. Dong, M. Yang, H. Zeng, G. Zou, Z. Lin, *Dalton Trans.* **2019**, *48*, 17451–17455.
[26] G. Blasse, B. C. Grabmaier, *Luminescent Materials.* Springer, Berlin **1994**.
[27] W. M. Yen, S. Shionoya, H. Yamamoto, *Phosphor Handbook*, CRC Press, Boca Raton **2006**.
[28] a) L.-J. Xu, H. Lin, S. Lee, C. Zhou, M. I Worku, M. Chaaban, Q. He, A. Plaviak, X. Lin, B. Chen, M.-H. Du, B. Ma, *Chem. Mater.* **2020**, *32*, 4692–4698; b) C. Zhou, H. Lin, H. Shi, Y. Tian, C. Pak, M. Shatruk, Y. Zhou, P. Djurovich, M.-H. Du, B. Ma, *Angew. Chem. Int. Ed.* **2018**, *57*, 1021–1024; *Angew. Chem.* **2018**, *130*, 1033–1036.
[29] J. Koziskova, F. Hahn, J. Richter, J. Kožíšek, *Acta Chim. Slov.* **2016**, *9*, 136–140.
[30] O. V. Dolomanov, L. J. Bourhis, R. J. Gildea, J. A. K. Howard, H. Puschmann, *J. Appl. Crystallogr.* **2009**, *42*, 339–341.
[31] a) G. M. Sheldrick, *Acta Crystallogr. Sect. C* **2015**, *71*, 3–8; b) G. M. Sheldrick, *Acta Crystallogr. Sect. A* **2008**, *64*, 112–122.
[32] DIAMOND Version 4.2.2 – *Crystal and Molecular Structure Visualization*, Crystal Impact GbR, Bonn, **2016**.
[33] a) A. L. Spek, *Acta Crystallogr. Sect. C* **2015**, *71*, 9–18; b) A. L. Spek, *Acta Crystallogr. Sect. D* **2009**, *65*, 148–155.
[34] J. C. de Mello, H. F. Wittmann, R. H. Friend, *Adv. Mater.* **1997**, *9*, 230–232.

Manuscript received: April 22, 2021
Revised manuscript received: June 14, 2021
Accepted manuscript online: June 15, 2021

ARTICLE

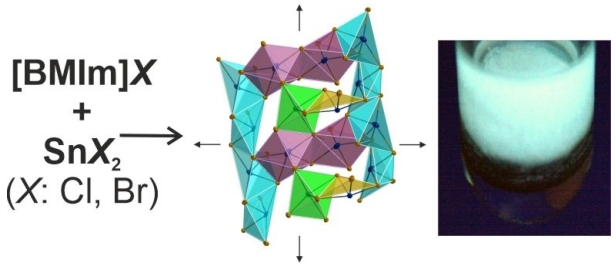

*Dr. M. Liebertseder, Dr. S. Wolf, Prof. Dr. C. Feldmann**